Supporting information:

Boosting of Oxygen Evolution Reaction Performance through Defect and Lattice Distortion Engineering

Zhijing Wu, [a] Jianwei Wang, [a] Haiyan Li, [a] Lixin Cao,*[a] and Bohua Dong *[a]

[a]School of Materials Science and Engineering, Ocean University of China, 238 Songling Road, Qingdao, 266100 P. R. China.

**Corresponding authors' Emails: caolixin@ouc.edu.cn (L. Cao) and dongbohua@ouc.edu.cn (B. Dong)*

Faradic efficiency. The evolved O_2 was collected by a water-gas displacing method. The i-t curve measured at the same time was integrated to get the cumulative charge (Q(C)). The volume of O_2 (V(mL)) was calculated through the relation of $V(mL)=Q(C)\times22.4(L\ mol^{-1})\times1000\div(F(C\ mol^{-1})\times4)$, where F means Faradic constant with a value of 96485 C mol^{-1}.

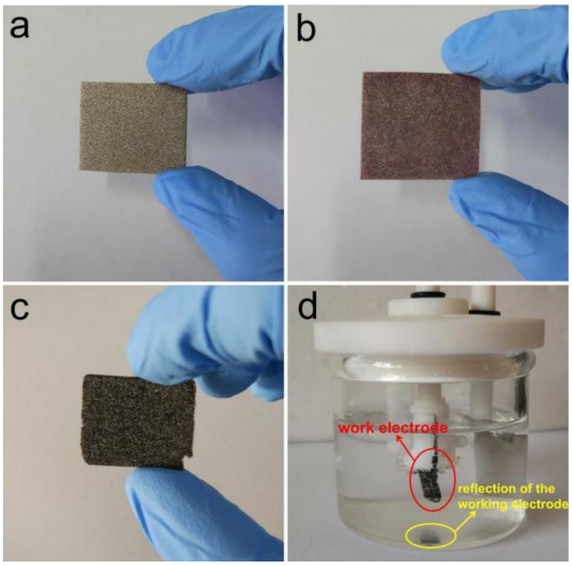

Figure S1. Digital images of a) bare NF, b) $Co(OH)_2$//NF, c) after high-heat sulfuration, d) electrolytic OER catalytic process

Figure S1 presents digital images of the bare Ni foam, $Co(OH)_2$//NF, after Co_9S_8/Ni_3S_2 growth, and electrolytic OER catalytic process. The initial color of the Ni foam electrode was brown (Figure S1a), and NF is surrounded closely and uniformly by the $Co(OH)_2$ (Figure S1b). After the Co_9S_8/Ni_3S_2 had grown on the Ni foam substrate, the foam surface became completely black (Figure S1c). Seeing from the change of color, we can observe the uniform and complete formation of Co_9S_8/Ni_3S_2 on the Ni foam, with no uncovered parts on the Ni foam substrate, which is further observed in the SEM images (Figure 2b). The uniform and complete morphology feature also have a tremendous effect on the performance of samples. Importantly, NF can still maintain stability and mechanical property after high temperature annealing at 550°C in Figure S1c and d, which had been proved by the chronoamperometry and multi-step chronopotentiometric curve.

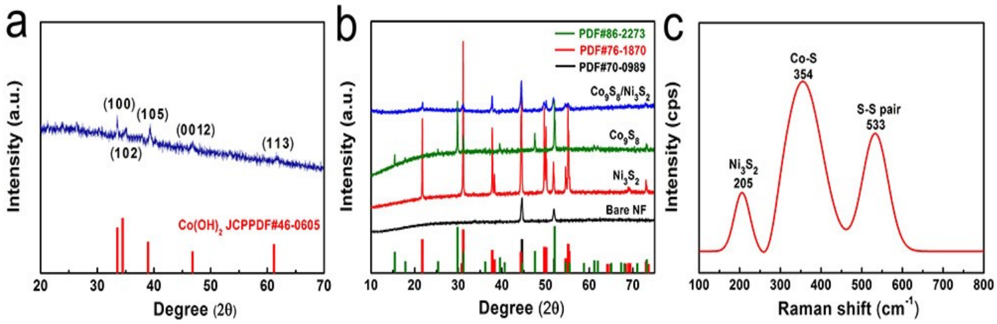

Figure S2. XRD patterns of a) $Co(OH)_2$, b) the bare NF, Co_9S_8, Ni_3S_2//NF, and Co_9S_8/Ni_3S_2 HNA//NF, c) Raman spectra of Co_9S_8/Ni_3S_2 HNA//NF.

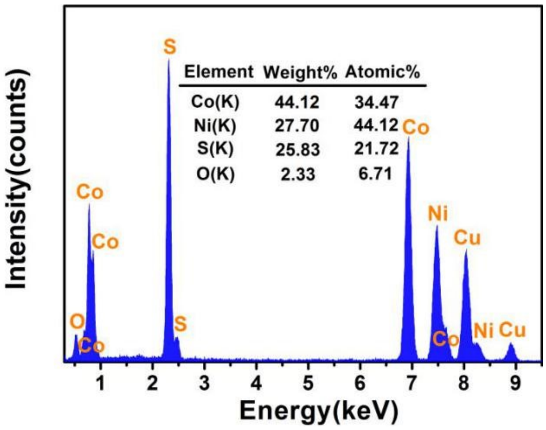

Figure S3. EDS spectrum of a single Co_9S_8/Ni_3S_2 nanowire. The Cu peaks in the EDS spectrum come from the Cu grid as sample holder.

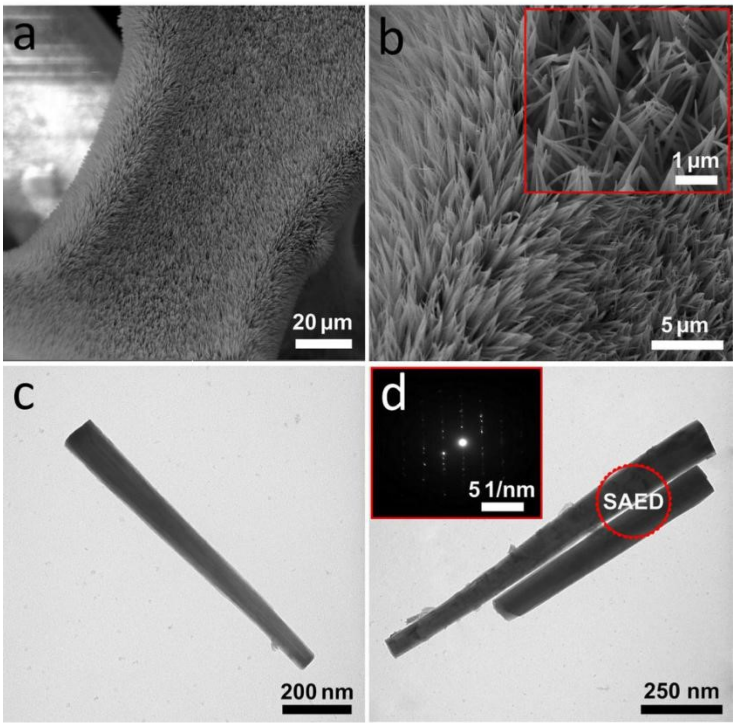

Figure S4. a,b) SEM images of $Co(OH)_2$ nanowires, c,d) TEM images of $Co(OH)_2$ nanowires. The inset is the selected-area electron diffraction (SAED) pattern of $Co(OH)_2$ nanowires.

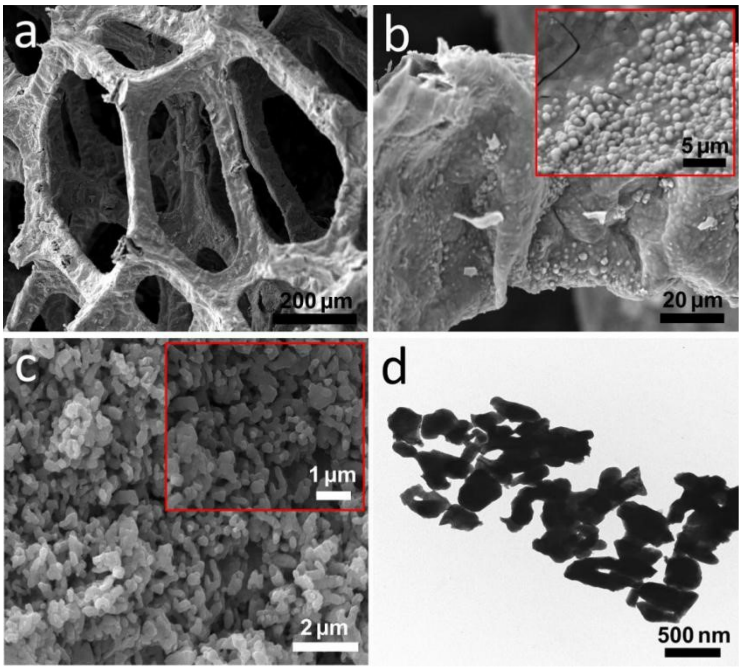

Figure S5. a,b) SEM images of Ni_3S_2//NF. c,d) SEM and TEM images of Co_9S_8 powder respectively.

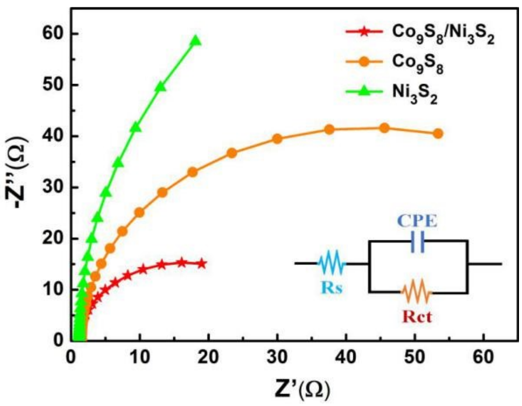

Figure S6. Nyquist plots of the Co_9S_8//NF, Ni_3S_2//NF, Co_9S_8/Ni_3S_2 HNA//NF. The inset is the equivalent circuit model that contains the electrolyte resistance (R_s), charge-transfer resistance (R_{ct}) and constant phase element (CPE).

Table S1. Electrochemical impedance spectroscopy (EIS) fitting results for Co_9S_8/Ni_3S_2 HNA//NF, Co_9S_8//NF and Ni_3S_2//NF.

materials	R_s (Ω)	R_{ct} (Ω)
Co_9S_8/Ni_3S_2 HNA//NF	**1.27**	**30**
Co_9S_8//NF	**1.57**	**83**
Ni_3S_2//NF	**1.19**	**219**

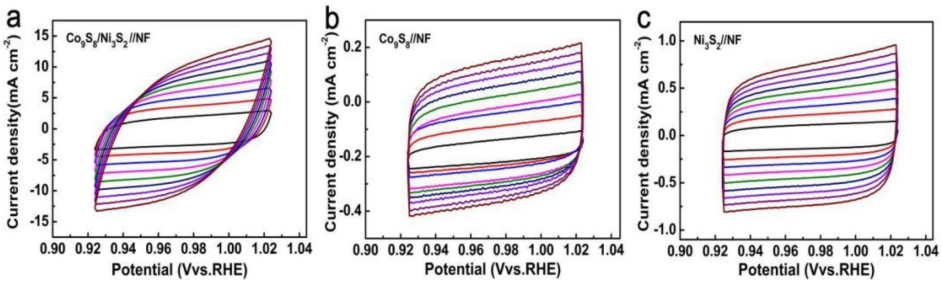

Figure S7. a,b,c) CV curves at different scan rates from 20, 40, 60 to 180 mV s^{-1} of the Co_9S_8/Ni_3S_2 HNA//NF, Co_9S_8//NF, Ni_3S_2//NF, respectively.

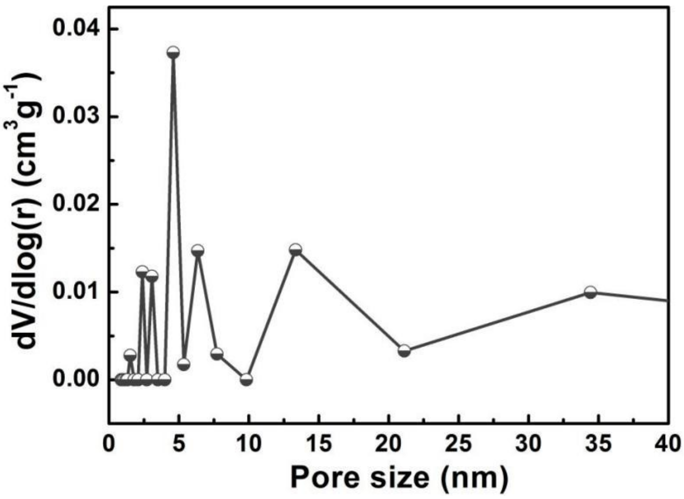

Figure S8. the BJH pore size distribution of the Co_9S_8/Ni_3S_2 HNA.

Table S2. The theoretical values, measured values and the Faradaic efficiencies of the amount of O_2 production at different periods.

Time (min)	10	20	30	40	50	60
Calculated O_2 (mmol)	0.08036	0.16072	0.24108	0.31697	0.38393	0.45089
Measured O_2 (mmol)	0.08000	0.15715	0.23126	0.30135	0.36608	0.42992
Faradaic efficiency (%)	100	97.78	95.93	95.07	95.35	95.35
Average (%)			**96.51**			

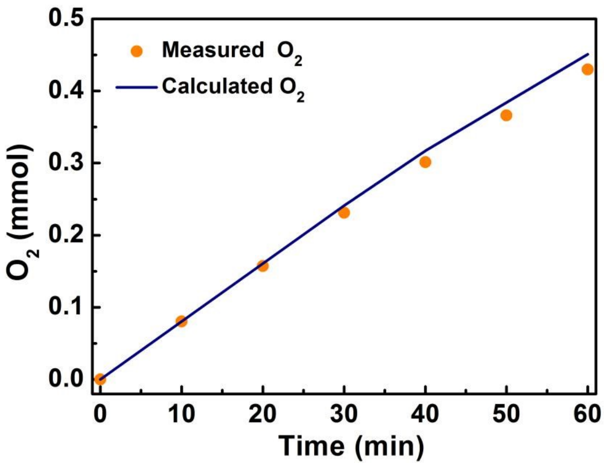

Figure S9. The experimental O_2 production versus theoretical quantities for OER water splitting of Co_9S_8/Ni_3S_2 HNA//NF at the constant current density.

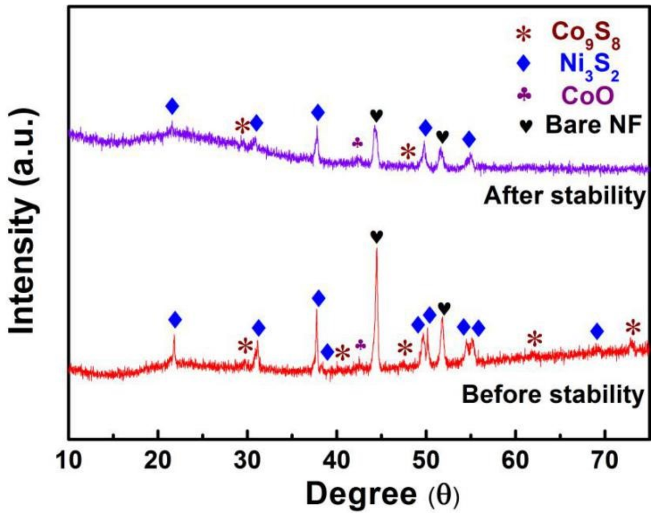

Figure S10. XRD patterns of Co_9S_8/Ni_3S_2 HNA//NF before and after stability.

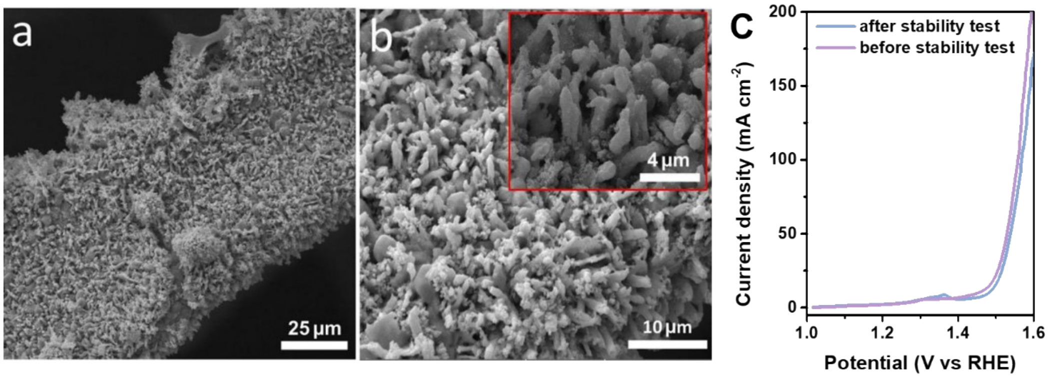

Figure S11. a, b) SEM images of Co_9S_8/Ni_3S_2 HNA//NF after OER stability measurments. (c) OER polarization curves of Co_9S_8/Ni_3S_2 HNA//NF before and after stability test.

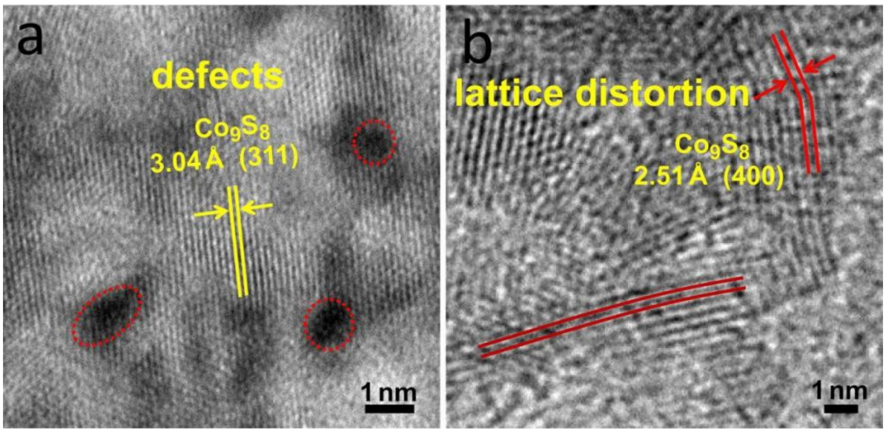

Figure S12. a, b) HRTEM images of Co_9S_8/Ni_3S_2 HNA//NF after harsh OER.

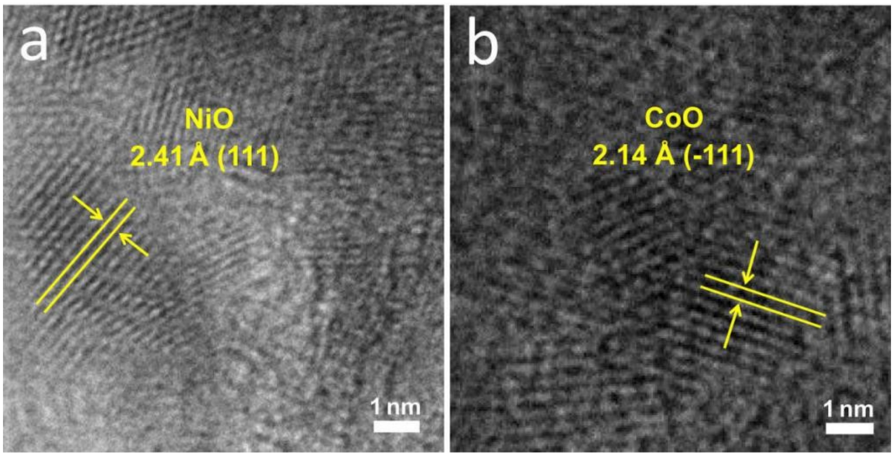

Figure S13. a, b) HRTEM images of Co_9S_8/Ni_3S_2 HNA//NF after harsh OER.

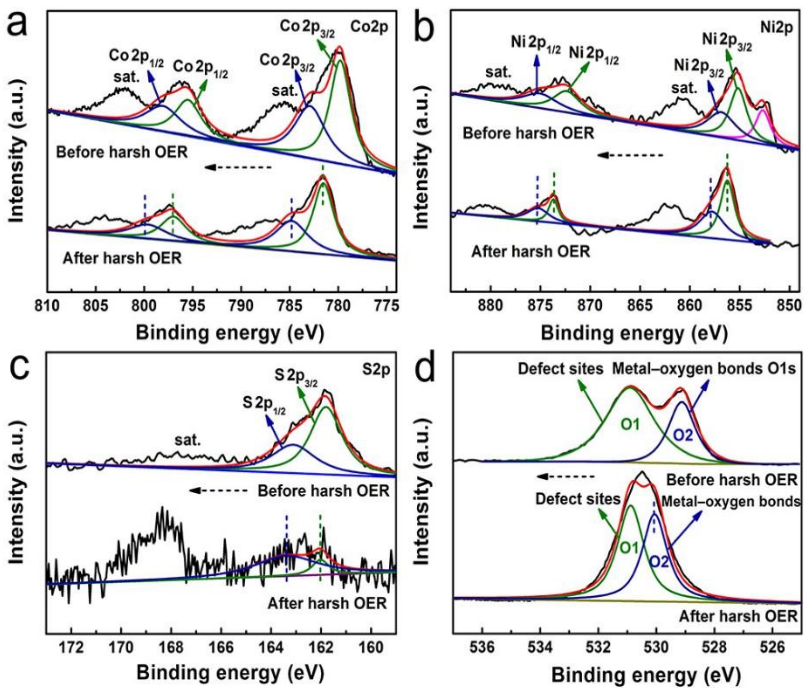

Figure S14. XPS spectra of a) Co 2p, b) Ni 2p, c) S 2p, and d) O 1s for Co_9S_8/Ni_3S_2 HNA//NF before and after harsh OER (Sat. means shake-up satellites)

Table S3. Comparison of OER performance based on non-precious metal electrocatalysts in alkaline electrolytes.

Materials	Electrolyte	η [mV] for j_{OER}= 10 mA cm^{-2}	Tafel slope [mV dec^{-1}]	References
Co_9S_8/Ni_3S_2 HNA//NF	**1.0 M KOH**	**223**	**79**	**This work**
NiS_2/CoS_2-O NWs	1.0 M KOH	235	31	7
Co_3O_4/N-rmGO//NF	0.1 M KOH	310	67	8
NiCoP//NF	1.0 M KOH	280	87	10
$NiCo_2S_4$ NWs//NF	1.0 M KOH	260	40	38
Ni_2P NPs	1.0 M KOH	290	59	S1
$Ni_{0.9}Fe_{0.1}$/NC	1.0 M KOH	330	45	S2
$Fe_6Ni_{10}O_x$	1.0 M KOH	286	48	S3
$Fe_{0.1}$-NiS_2 NA//Ti	1 .0M KOH	η_{100} =231	43	S4
NiCoP/C nanoboxes	1.0 M KOH	330	96	S5
Cu@CoS_x//CF	1.0 M KOH	270	-	S6
NiCoP nanosheet	1.0 M KOH	η_{50}=310	68.6	S7
NiS//NF	1.0 M KOH	η_{20}=335	89	S8
$NiCo_2S_4$ NA//CC	1.0 M KOH	η_{100}=340	89	S9
Co_3O_4@CoS//NF	1.0 M KOH	290	77.6	S10
$Ni(OH)_2$-TCNQ//CF	1.0 M KOH	η_{20}=225	110	S11
SnCoFe-Ar//NF	1.0 M KOH	270	42.3	S12
$Zn_{0.15}Ni_{0.85}Co_2O_4$	0.1 M KOH	560	62	S13
$Co_{0.7}Fe_{0.3}P$//CNT	1.0 M KOH	243	36	S14
Co-MOF nanosheet	1.0 M KOH	263	74	S15
$NiMoO_{4-x}/MoO_2$	1.0 M KOH	320	69	S16

References

S1.Stern, L.-A.; Feng, L.; Song, F.; Hu, X., Ni_2P as a Janus Catalyst for Water Splitting: the Oxygen Evolution Activity of Ni_2P Nanoparticles. *Energy Environ. Sci.* 2015, 8, 2347-2351.

S2.Zhang, X.; Xu, H.; Li, X.; Li, Y.; Yang, T.; Liang, Y., Facile Synthesis of Nickel-Iron/Nanocarbon Hybrids as Advanced Electrocatalysts for Efficient Water Splitting. *ACS Catal.* 2016, 6, 580-588.

S3.Kuai, L.; Geng, J.; Chen, C.; Kan, E.; Liu, Y.; Wang, Q.; Geng, B., A Reliable Aerosol-Spray-Assisted Approach to Produce and Optimize Amorphous Metal Oxide Catalysts for Electrochemical Water Splitting. *Angew. Chem. Int. Ed.* 2014, 53, 7547-7551.

S4.Yang, N.; Tang, C.; Wang, K.; Du, G.; Asiri, A. M.; Sun, X., Iron-doped Nickel Disulfide Nanoarray: A Highly Efficient and Stable Electrocatalyst for Water Splitting. *Nano Res.* 2016, 9, 3346-3354.

S5.He, P.; Yu, X.-Y.; Lou, X. W., Carbon-Incorporated Nickel-Cobalt Mixed Metal Phosphide Nanoboxes with Enhanced Electrocatalytic Activity for Oxygen Evolution. *Angew. Chem. Int. Ed. Engl.* 2017, 56, 3897-3900.

S6.Liu, Y.; Li, Q.; Si, R.; Li, G.-D.; Li, W.; Liu, D.-P.; Wang, D.; Sun, L.; Zhang, Y.; Zou, X., Coupling Sub-Nanometric Copper Clusters with Quasi-Amorphous Cobalt Sulfide Yields Efficient and Robust Electrocatalysts for Water Splitting Reaction. *Adv. Mater.* 2017, 29, 1606200.

S7.Li, Y.; Zhang, H.; Jiang, M.; Kuang, Y.; Sun, X.; Duan, X., Ternary NiCoP Nanosheet Arrays: An Excellent Bifunctional Catalyst for Alkaline Overall Water Splitting. *Nano Res.* 2016, 9, 2251-2259.

S8.Zhu, W.; Yue, X.; Zhang, W.; Yu, S.; Zhang, Y.; Wang, J.; Wang, J., Nickel Sulfide Microsphere Film on Ni Foam as an Efficient Bifunctional Electrocatalyst for Overall Water Splitting. *Chem. Commun.* 2016, 52, 1486-1489.

S9.Liu, D.; Lu, Q.; Luo, Y.; Sun, X.; Asiri, A. M., $NiCo_2S_4$ Nanowires Array as an Efficient Bifunctional Electrocatalyst for Full Water Splitting with Superior Activity. *Nanoscale* 2015, 7, 15122-15126.

S10.Zhou, J.; Dou, Y.; Zhou, A.; Guo, R.-M.; Zhao, M.-J.; Li, J.-R., MOF Template-Directed Fabrication of Hierarchically Structured Electrocatalysts for Efficient Oxygen Evolution Reaction. *Adv. Energy Mater.* 2017, 7, 1602643.

S11.Guo, X.; Kong, R.-M.; Zhang, X.; Du, H.; Qu, F., $Ni(OH)_2$ Nanoparticles Embedded in Conductive Microrod Array: An Efficient and Durable Electrocatalyst for Alkaline Oxygen Evolution Reaction. *ACS Catal.* 2018, 8, 651-655.

S12.Chen, D.; Qiao, M.; Lu, Y.-R.; Hao, L.; Liu, D.; Dong, C.-L.; Li, Y.; Wang, S., Preferential Cation Vacancies in Perovskite Hydroxide for the Oxygen Evolution Reaction. *Angew. Chem. Int. Ed.* 2018, 57, 8691-8696.

S13.Yang, M.; Li, Y.; Yu, Y.; Liu, X.; Shi, Z.; Xing, Y., Self-Assembly of Three-Dimensional Zinc-Doped $NiCo_2O_4$ as Efficient Electrocatalysts for Oxygen Evolution Reaction. *Chem. Eur. J* 2018, 24, 13002-13008.

S14.Zhang, X.; Zhang, X.; Xu, H.; Wu, Z.; Wang, H.; Liang, Y., Iron-Doped Cobalt Monophosphide Nanosheet/Carbon Nanotube Hybrids as Active and Stable Electrocatalysts for Water Splitting. *Adv. Funct. Mater.* 2017, 27, 1606635.

S15.Xu, Y.; Li, B.; Zheng, S.; Wu, P.; Zhan, J.; Xue, H.; Xu, Q.; Pang, H., Ultrathin Two-dimensional Cobalt–organic Framework Nanosheets for High-performance Electrocatalytic Oxygen Evolution. *J. Mater. Chem. A* 2018, 6, 22070-22076.

S16.Zhang, Z.; Ma, X.; Tang, J., Porous $NiMoO_{4-x}/MoO_2$ Hybrids as Highly Effective Electrocatalysts for the Water Splitting Reaction. *J. Mater. Chem. A* 2018, 6, 12361-12369.